Actively Controlled Ionic Current Gating In Nanopores

Samuel Bearden[1], Guigen Zhang[1,2,3*]
[1]Department of Bioengineering,
[2]Department of Electrical and Computer Engineering,
[3]Institute for Biological Interfaces of Engineering,
Clemson University, 301 Rhodes Research Center, Clemson, SC 29634-0905
* guigen@clemson.edu

Abstract: A conical nanopore was developed that allowed the ionic current to be gated by external application of electrical potential. A numerical model of the pore was created in COMSOL to elucidate the mechanism of action in this pore. The model is composed of a conical nanopore geometry with a gold-plated Si_3N_4 structure and a complete Gouy-Chapman-Stern electrical double layer. The Poisson, Nernst-Planck, and Navier-Stokes equations were solved over the axisymmetric model geometry. Overlap in the diffuse layer caused the pore to be ion selective. Biasing the gold layer of the pore created regions of opposing ion selectivity responsible for the non-conducting state of the pore. Current in the conducting state was mediated by electrophoresis with negligible electroosmosis. This study demonstrates a pore whose conductive properties may be externally controlled in real-time.

Keywords: Nanopore, Gating, Nanoelectrofluidics, Ionic Transistor, COMSOL

1. Introduction

Nanopores have been identified as a key structure for the next generation of biosensors and DNA sequencers. [1] The very small sampling volume for these types of sensors allows sub-molecular resolution. To facilitate further development of these devices, it is necessary to understand the fundamental physical mechanisms associated with these structures.

The flow of ionic solutions through nanopores is subject to unexpected behaviors due to their very small size and interactions between the pore materials and the fluid. Such behaviors include electroosmotically enhanced flow through carbon nanotubes and current rectification in conical nanopores. [2–4] Often the effects seen in nanopore are due to overlap in the diffuse region of the electrical double layer. In carbon nanotubes, the overlap of the diffuse layer creates a region of net charge that results in enhanced electroosmotic and electrophoretic current. [3]

Similarly, rectified ionic current has been produced in conical nanopores by chemically modifying the pore surface with charged species. [5–7] In these types of modified nanopores, the rectification of ionic current is controlled by modulating the pH of the solution about the isoelectric point of the surface bound species. The resulting ionic current preferentially travels in one direction in response to an externally applied electric field. Because chemically controlled gating requires physically altering the pH of the solution or modifying the bound species, a different method of control is desirable. Electrical control and electrical boundary conditions (such as material work functions and the Gouy-Chapman-Stern electrical double layer) have largely been neglected in the study of nanopores. By exploiting the naturally occurring surface potentials and externally applying biases to the surface of a nanopore, we were able to actively control the conductance and induce actual gating behavior in a solid-state conical nanopore.

2. Governing Equations

$$\nabla^2 V = -\frac{\rho_c}{\varepsilon_0 \varepsilon_r} \qquad \text{(1) Poisson's Equation}$$

$$\nabla \cdot \left(-D_j \nabla c_j - z_j \mu_{m,j} F c_j \nabla V \right) + u \cdot \nabla c_j = R_j$$
$$N_j = -D_j \nabla c_j - z_j \mu_{m,j} F c_j \nabla V + u c_j$$
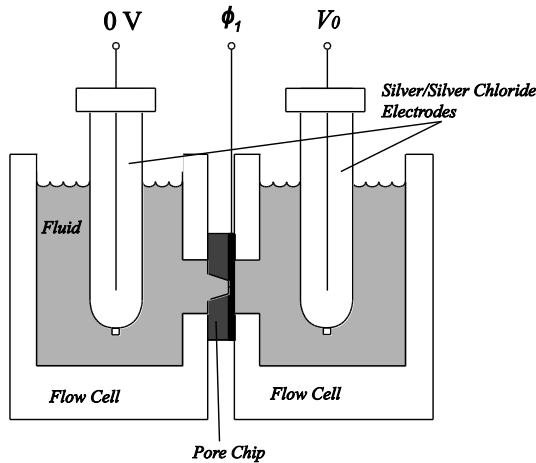$$\text{(2) Nernst-Plank Equation}$$

$$\rho_V\left(u\cdot\nabla\right)u = \nabla\cdot\left[-PI+\gamma\left(\nabla u+\left(\nabla u\right)^T\right)-\frac{2}{3}\gamma\left(\nabla\cdot u\right)I\right]+\vec{F}_V$$

$$\nabla\cdot\left(\rho_V u\right)=0$$

(3) Stokes Equation
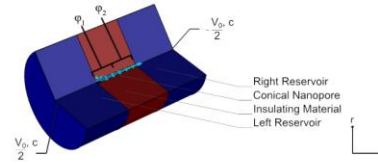

Figure 2. The axisymmetric conical geometry of the pore model.

3. Methods

A nanopore was formed by focused ion beam in a thin membrane of Si_3N_4 and gold on a silicon chip. The nanopore chip was placed in a flow cell (Figure 1) where the cross-pore current could be measured under constant cross-membrane potential. Cross-membrane potential and current were monitored by an Axopatch 200B patch clamp system. The gold layer was biased via an external potentiometer in steps of 200 mV.

Figure 1. The flow cell/nanopore chip system used for all experimental measurements.

An axisymmetric model of the nanopore was developed (Figure 2). The nanopore consisted of Si_3N_4 and gold layers, with the small end of the conical geometry oriented within the gold layer. An aqueous electrolyte fluid was modeled within the nanopore and within reservoirs on either side of the nanopore membrane. At the interface of the pore wall and the solution, the Stern layer of the electrical double layer was modeled as a parallelogram with fixed thickness. In the rotated geometry, the Stern layer forms a conical shell at the pore wall.

The Poisson equation (1) was solved over the entire model. The only charges considered consisted of the ions in solution. The Stern layer was considered as a region of zero net charge. The electrical permittivity within the Stern layer smoothly transitions from the permittivity of the Si_3N_4 pore material to the permittivity of the solution. The smoothly varying permittivity was characterized by the equation:

$$\varepsilon = \frac{\varepsilon_s - \varepsilon_p}{1+\exp\left(gr-h\right)}+\varepsilon_p$$

where ε_p is the permittivity of the pore material and ε_s is the permittivity of the solution. Potential was applied across the nanopore membrane (V_0) and on the gold layer (φ_1).The cross-pore potential was held constant and the applied bias (φ_1) was swept from -0.6 V to 0.6 V. The work function potential of the Si_3N_4 layer was considered as a surface potential at the interface of the Si_3N_4 and fluid (φ_2).

The Nernst-Planck (2) and Navier-Stokes (3) equations were solved over the fluid domain. The concentration and diffusion coefficients of the ions in solution were defined according to experimental conditions (as a 100 mM KCl solution). The concentration of the solution was fixed at the far ends of the fluid reservoirs. A volume force was applied to the fluid through coupling of the Navier-Stokes and Nernst-Planck equation via the relation ($\vec{F}_V = F_c \sum^i\left(z_j c_j\right)\cdot\nabla V$). The boundary between the fluid and nanopore was non-slip.

4. Experimental Results and Discussion

The numerical conductance through the pore is shown in figure 3 along with experimental results. When the applied bias is negative, the conductance is positive and proportional to the applied bias. When the applied bias is negative, the conductance is very small (near zero). These calculated conductances closely resemble experimental results. It was found that varying the angle of the pore wall modulated the model conductance in a way consistent with the behaviour of the pore. Changing the wall angle in the model allowed us to find lower and upper bound on the conductance.
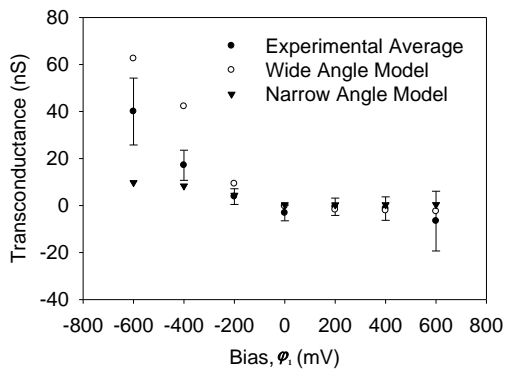

Figure 3. The gated conductance driven by the applied bias. The numerical results closely approximate the experimental results.

The conductance and gated state are produced by varying the polarity of the solution within the nanopore. Figure 4 shows the net polarity of the solution within the nanopore as a function of applied bias in the conducting and non-conducting states. When the applied bias is negative, a homogeneous net positive charge exists within the pore allowing current to pass. However, when the bias is positive, two distinct regions occur within the pore having opposite polarity. In the state of opposing polarity, the current is locked and no net current can be produced through the pore. Because the conducting state occurs when φ_1 is negative, it is possible to conclude that φ_2 must be negative.
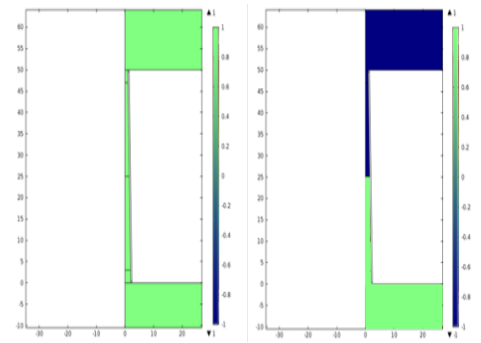

Figure 4. The polarity of the solution under negative bias (left) and positive bias (right) corresponding to conducting and gated conditions, respectively.

The net charge (and polarity) of the solution within the nanopore is a result of the electrical double layer. Figure 5 shows the concentration of the cation and anion as a function of distance from the centerline of the pore. Close to the wall the difference in ion concentration is greatest. At a distance from the wall, the difference in concentrations decrease until electroneutrality is achieved. The length at which the ions reach electroneutrality is the width of the diffuse layer of the electrical double layer. However, within the nanopore, which has a radius that is smaller than the width of the diffuse layer, electroneutrality is never achieved and the diffuse layer overlaps itself. Since the gating effect is a function of the electrical double layer overlap, which is in turn a function of pore radius, we may expect the gating effect to essentially disappear for pores of relatively large radius. Experimental pores of relatively large minimum diameter (100 nm - 200 nm) did not exhibit gating behavior.
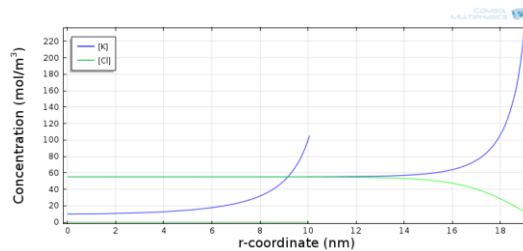

Figure 5. The relative concentrations of the cation and anion in the diffuse layer follow the expected trend within the nanopore near the small opening and large opening. The origin corresponds to the axis of symmetry of the pore. Note that electroneutrality is not reached within the pore.

In the conducting state, the current through the model is carried by an electrophoretic mechanism (Figure 6). Under negative bias, the current resembles the current expected based on the size of the pore and the solution conductivity. When the current is gated and the pore is in the non-conducting state (positive bias), the electrophoretic current is very small. Under all conditions, the electroosmotic current is very small. The electroosmotic current is ~10^5 times smaller than the electrophoretic current under every considered bias.
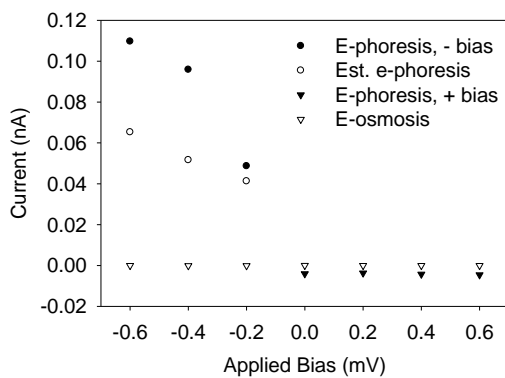
Figure 6. The current through this type of nanopore is driven by the electrophoretic mechanism. In the conducting state, the electrophoretic current resembles the empirically calculated current. Electroosmosis is negligible under all biases.

The magnitude of the conducting state current is driven by an electric field within the nanopore. Figure 7 shows the electric potential along the symmetry axis of the model. The unbiased (φ_2) region of the pore occurs between z = 0 nm and z = 125 nm, the biased (φ_1) region exists between z = 125 nm and 250 nm. The difference in potential between these regions cause an internal electric field to develop that is responsible for the proportionality between the ionic current and applied bias (φ_1). The electric field within the pore is independent of the cross membrane potential. The internal electric field is capable of driving the ionic current without an externally applied cross membrane potential. The magnitude and polarity of the internal electric field influences the diffuse layer of the electrical double layer, causing the characteristic behavior of the device.
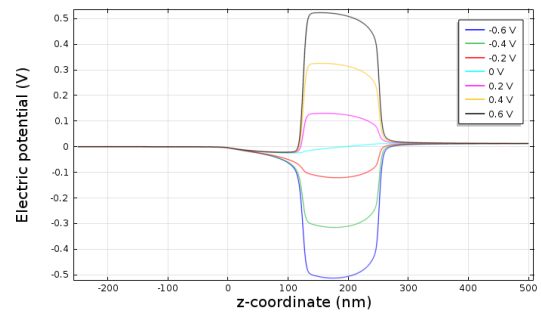
Figure 7. The electric potential along the axis of symmetry. The potential difference between the unbiased region (0 nm to 125 nm) and the biased region (125 nm to 250 nm) drives the ionic current in the conducting state of the device.

5. Conclusions

A conical gated nanopore was produced and modeled in COMSOL. The ionic conductance of the numerical pore model compared well to the experimental results. In the conducting state the current is carried by an electrophoretic mechanism. From the observed gating behavior, we can surmise that the current is carried primarily by positive ions and that the Si_3N_4 layer carries a negative surface potential. The gating effect is due to regions of differing polarity within the nanopore effectively locking the ionic current in a low conductance state. Such gating is only possible in pores whose radius is smaller than the width of the electrical double layer where overlap of the diffuse layer makes the pore ion selective. This study successfully demonstrates a method of actively controlling the gating and current characteristics of a nanopore.

6. References

[1]   Timp W, Mirsaidov UM, Wang D, Comer J, Aksimentiev A and Timp G 2010 *IEEE transactions on nanotechnology* [Internet] **9** 281–294 Available from: http://www.pubmedcentral.nih.gov/articlerender.fcgi?artid=3092306&tool=pmcentrez&rendertype=abstract

[2]   Pang P, He J, Park JH, Krstić PS and
        Lindsay S 2011 *ACS nano* [Internet] **5**
        7277–83 Available from:
        http://www.ncbi.nlm.nih.gov/pubmed/21
        888368

[3]   Bearden S and Zhang G 2013
        Nanotechnology [Internet] [cited 2013
        Apr 15];**24** 125204 Available from:
        http://www.ncbi.nlm.nih.gov/pubmed/23
        466571

[4]   Siwy ZS 2006 *Advanced Functional
        Materials* [Internet] [cited 2012 Mar
        8];**16** 735–746 Available from:
        http://doi.wiley.com/10.1002/adfm.2005
        00471

[5]   Apel PY, Korchev Y., Siwy Z, Spohr R
        and Yoshida M 2001 *Nuclear
        Instruments and Methods in Physics
        Research Section B: Beam Interactions
        with Materials and Atoms* [Internet] **184**
        337–346 Available from:
        http://linkinghub.elsevier.com/retrieve/pi
        i/S0168583X01007224

[6]   Siwy Z, Heins E, Harrell CC, Kohli P
        and Martin CR 2004 *Journal of the
        American Chemical Society* [Internet]
        126 10850–1 Available from:
        http://www.ncbi.nlm.nih.gov/pubmed/15
        339163

[7]   Ali M, Mafe S, Ramirez P, Neumann R
        and Ensinger W 2009 *Langmuir : the
        ACS journal of surfaces and colloids*
        [Internet] [cited 2012 May 25];**25**
        11993–7 Available from:
        http://www.ncbi.nlm.nih.gov/pubmed/19
        780595